



Deposited via The University of Leeds.

White Rose Research Online URL for this paper:

<https://eprints.whiterose.ac.uk/id/eprint/81224/>

Version: Accepted Version

---

**Article:**

Angus, DAC, Aljaafari, A, Usher, P et al. (2014) Seismic waveforms and velocity model heterogeneity: towards full-waveform microseismic location algorithm. *Journal of Applied Geophysics*, 111. 228 - 233. ISSN: 0926-9851

<https://doi.org/10.1016/j.jappgeo.2014.10.013>

---

**Reuse**

Items deposited in White Rose Research Online are protected by copyright, with all rights reserved unless indicated otherwise. They may be downloaded and/or printed for private study, or other acts as permitted by national copyright laws. The publisher or other rights holders may allow further reproduction and re-use of the full text version. This is indicated by the licence information on the White Rose Research Online record for the item.

**Takedown**

If you consider content in White Rose Research Online to be in breach of UK law, please notify us by emailing [eprints@whiterose.ac.uk](mailto:eprints@whiterose.ac.uk) including the URL of the record and the reason for the withdrawal request.

# 1 **Seismic waveforms and velocity model**

## 2 **heterogeneity: Towards a full-waveform**

### 3 **microseismic location algorithm.**

4 D.A. Angus<sup>1</sup>, A. Aljaafari<sup>2</sup>, P. Usher<sup>3</sup>, and J.P. Verdon<sup>3</sup>

5 <sup>1</sup> Centre for Integrated Petroleum Engineering & Geoscience, University of Leeds, UK ([d.angus@leeds.ac.uk](mailto:d.angus@leeds.ac.uk))

6 <sup>2</sup> School of Earth & Environment, University of Leeds, UK

7 <sup>3</sup> Department of Earth Sciences, University of Bristol, UK

## 8 **ABSTRACT**

9 Seismic forward modeling is an integral component of microseismic location  
10 algorithms, yet there is generally no one correct approach, but rather a range of  
11 acceptable approaches that can be used. Since seismic signals are band limited, the  
12 length scale of heterogeneities can significantly influence the seismic wavefronts and  
13 waveforms. This can be especially important for borehole microseismic monitoring,  
14 where subsurface heterogeneity can be strong and/or vary on length scales  
15 equivalent to or less than the dominant source wavelength. In this paper, we show  
16 that ray-based approaches are not ubiquitously suitable for all borehole microseismic  
17 applications. For unconventional reservoir settings, ray-based algorithms may not be  
18 suitably accurate for advanced microseismic imaging. Here we focus on exploring the  
19 feasibility of using one-way wave equations as forward propagators for full waveform  
20 event location techniques. As a feasibility study, we implement an acoustic wide-  
21 angle wave equation and use a velocity model interpolation approach to explore the  
22 computational efficiency and accuracy of the solution. We compare the results with  
23 an exact solution to evaluate travel-time and amplitude errors. The results show that  
24 accurate travel-times can be predicted to within 2 ms of the true solution for modest  
25 velocity model interpolation. However, for accurate amplitude prediction or for higher

1 dominant source frequencies, a larger number of velocity model interpolations is  
2 required.

### 3 **1. Introduction**

4 Microseismic monitoring is being applied increasingly in the hydrocarbon industry  
5 and this is because it provides a means of remotely monitoring the state of stress  
6 (i.e. failure) within the subsurface. Microseismic technology enables monitoring  
7 hydraulic fracture programs in unconventional reservoirs, assessment of fault  
8 reactivation and hydrocarbon leakage in conventional reservoirs, as well as  
9 characterization of the subsurface rock mass (e.g., frequency dependent seismic  
10 anisotropy). Although there has been significant development of advanced  
11 microseismic attributes (commonly referred to as ‘beyond the dots in the box’ by  
12 Eisner et al., 2010a), the location of microseismic events (the ‘dots’) represent the  
13 most fundamental measurement in microseismic monitoring (e.g., Eisner et al.,  
14 2010b).

15 Ray based solutions, such as eikonal solvers, are very attractive since they provide  
16 computationally fast solutions. If first-order effects of material averaging (or wavefront  
17 smoothing) can be modelled by a gradually varying medium and the wave path  
18 lengths are not too great, then basic ray methods should be applicable (e.g.,  
19 Cerveny, 2001). However, ray based approaches are approximate solutions and do  
20 not accurately model wave phenomena when velocity heterogeneity varies on length  
21 scales on the order of or less than the dominant seismic wavelength (e.g., Cerveny,  
22 2001; Angus, 2014). For instance, if strong multiple scattering or wide-angle  
23 diffraction is important, where seismic energy is scattered away from the direct ray  
24 path yet in the forward direction within the Fresnel zone, a numerical solution of the

1 full wave equation is necessary (e.g., Thomson, 1999; Carcione et al., 2002). Full  
2 waveform approaches, such as finite-difference solvers, yield substantially more  
3 accurate solutions, but at the expense of slower computation times (e.g., Thomson,  
4 1999). These full waveform solutions will yield very accurate solutions but, more  
5 often than not, may not be practical for microseismic processing. Thus, selecting an  
6 appropriate method involves weighing the advantages and disadvantages of all  
7 acceptable approaches in terms of accuracy requirements and computational  
8 limitations.

9 Usher et al. (2013) showed that microseismic waveforms are sensitive to velocity  
10 model and microseismic source frequency (this is fundamental to the physics wave  
11 propagation of bandlimited signals, i.e., frequency dependence of wave propagation).  
12 This dependence on velocity model and source frequency as well as unavoidable  
13 uncertainty in true velocity model will impact on the accuracy of microseismic event  
14 locations and hence reliability of any geometrical interpretation (Thornton, 2013). For  
15 instance, Thornton (2013) compared microseismic travel-time predictions between an  
16 acoustic eikonal solver and a finite-difference solver, and observed noticeable  
17 mismatch between the two solutions. The results from Thornton (2013) are  
18 consistent with Usher et al. (2013) in that wave propagation is sensitive to velocity  
19 model heterogeneity, and that certain ray based approaches, being limited to  
20 smoothly varying velocity models, may not be universally suitable in all  
21 unconventional hydrocarbon settings. Ray based approaches neglect frequency-  
22 dependent effects and non-geometrical arrivals (e.g., head waves), and are generally  
23 only suitable for smooth velocity models (i.e., when heterogeneity length scales are  
24 greater than the dominant seismic wavelength).

1 In this paper, we explore the feasibility of using the wide-angle one-way wave  
2 equation as a forward propagator (i.e., Green's function) for microseismic event  
3 location. The wide-angle one-way wave equation is capable of modeling the  
4 waveform evolution along the underlying wavefront, where frequency dependent  
5 effects and non-geometrical arrivals can be predicted. We focus on borehole  
6 microseismic monitoring geometry, where wave propagation is predominantly sub-  
7 horizontal. In such circumstances, the influence of non-geometrical arrives due to  
8 horizontal layering as well as other wave phenomena due to velocity heterogeneity  
9 on lengths scales on the order of or less than the dominant seismic wavelength will  
10 be significant. For surface microseismic monitoring, the influence of vertical velocity  
11 variation is less problematic and so ray-based methods should be appropriate.

## 12 **2. Theory**

### 13 **2.1 The influence of Green's function on event location error**

14 To highlight the impact of velocity model and bandlimited wave propagation on  
15 microseismic waveforms and hence on event location uncertainty, we evaluate the  
16 influence of velocity model heterogeneity on event location using a ray-based  
17 location algorithm. Specifically, we use an eikonal solver to generate a look-up table  
18 for P- and S-wave travel-times through three depth-dependent 2D velocity models,  
19 thereby providing more realistic estimates of location error. A total of nine synthetic  
20 datasets are generated (Usher et al., 2013) by varying the velocity model and event  
21 dominant source frequency: three velocity models (3 layer surface seismic, 13 layer  
22 VSP and 34 layer sonic velocity models) and three geometrically equivalent  
23 microseismic events but with different dominant source frequencies (40 Hz, 150 Hz  
24 and 300 Hz). To generate the full waveform synthetics, we use the full waveform E3D

1 code (Larsen and Harris, 1993). E3D is a staggered grid, fourth-order accurate in  
2 space and second-order accurate in time finite-difference algorithm (e.g., Virieux,  
3 1984; 1986) for isotropic two-dimensional (2D) and three-dimensional (3D)  
4 viscoelastic media. The specific eikonal solver used was developed as part of the  
5 Madagascar package (Sethian, 1996; Sethian and Popovici, 1999). The eikonal  
6 solver is used to generate a look-up table of travel-times from each point in a  
7 discretized velocity model to each receiver. The optimum event location and  
8 uncertainty is evaluated using the neighbourhood algorithm of Sambridge (1999a,b).  
9 The root-mean-square misfit between observed travel-time from the full waveform  
10 synthetic seismograms and the predicted travel-time from the ray-base eikonal solver  
11 is the objective function that is minimized. Since the eikonal solver produces travel-  
12 times for discrete points in the subsurface and the neighbourhood algorithm requires  
13 the computation of a continuously varying hyper-surface, we use the interpolation  
14 algorithm of (Akima, 1978) to compute travel-times for points between the discretized  
15 grid of the eikonal solver.

16 In figure 1, we compare the influence of velocity model on event location for a  
17 microseismic source with dominant frequency 300 Hz (the results for lower dominant  
18 frequencies are similar). In this comparison, finite-difference synthetic microseismic  
19 waveforms are generated for three velocity models (3 layer surface seismic model,  
20 VSP and sonic log). The travel-times of the P- and S-waves are picked manually for  
21 each waveform data set. Locations for each of these sets of picks were computed  
22 using an eikonal solver using each of the three velocity models, giving a total of 9  
23 permutations (3 velocity models used to generate synthetic data and 3 velocity  
24 models used in the event location algorithm). The resulting event locations are listed  
25 in Table 1.

1 [Figure 1 here]

2 First we consider the cases where the velocity model used to generate the synthetic  
3 data and the velocity model used to locate the events are identical (light blue,  
4 medium grey and dark red dots in Figure 1). These results indicate the accuracy of  
5 the location algorithm, as any mislocation will come either from errors in picking, or  
6 from limitations in the use of eikonal solvers to compute travel-times: for instance,  
7 eikonal solvers compute the first arrival travel-time, regardless of whether this arrival  
8 is the most energetic arrival. For this case the locations are to within  $\pm 5$  m in depth.  
9 The horizontal distances range between 10 m and 40 m away from the modelled  
10 source location and this is due to the effects of array geometry; we use a single  
11 vertical borehole in this case. Using one or more additional boreholes would improve  
12 the horizontal location misfit (e.g., Jones et al., 2014). Note that for the sonic log  
13 model (dark red dot in Figure 1), the confidence ellipse is larger indicating that the  
14 eikonal solver is yielding less accurate results as expected given that the model  
15 heterogeneity is beyond the ray theory high-frequency assumption. Next, we  
16 consider the cases where one velocity model has been used to generate the full  
17 waveform synthetic data, but the locations are computed using a different, and  
18 therefore incorrect, velocity model. The estimated source depths range between 5 m  
19 and 30 m of the true source depth, whereas the estimated source lateral locations  
20 range between 10 to 90 m from the true source lateral location. This suggests there is  
21 an error due to using different velocity models on the order of 10 m. We should note  
22 that this error is very optimistic (i.e., best case scenario) and we would expect error in  
23 real data to be larger, and this is because the synthetic waveforms are clean from  
24 typical microseismic noise.

25 [Table 1 here]

## 2.2 Beyond ray-based algorithms – wide-angle one-way wave equation

Ray based forward modeling algorithms are extremely pervasive throughout the hydrocarbon industry because they provide very efficient travel-time predictions for a range of problems, such as velocity model building (e.g., Jones 2010) and event locations (e.g., Maxwell 2014). However, ray theory is a high-frequency approximate solution to the wave equation (Cerveny 2001) and care must be taken when applying ray-based approaches to unconventional environments. Implicit in ray theory is the assumption that the velocity model heterogeneity is smoothly varying with respect to the length scales of the seismic wave. For microseismic events, assuming dominant frequencies ranging between tens of Hz up to hundreds of Hz (e.g., Gibowicz and Kijko, 1994; Trifu et al., 2000; Teanby et al., 2004; Rentsch et al., 2007; Maxwell, 2014), the wavelength of microseismic waves can range on the order of 100s of meters for low frequency events down to 10s of meters or less for higher frequency sources. For moderate to high frequency events (e.g., between 100 to 500 Hz signals), vertical velocity heterogeneity can be significant enough such that the ray theory assumption of smoothly varying velocity breaks-down (Thornton, 2013). This is especially problematic for borehole arrays since the velocity heterogeneity varies across the sub-horizontally propagating wavefront (Figure 1). However, vertical heterogeneity also impacts surface array imaging, such as degrading imaging aperture (e.g., Price, 2013).

The one-way wave equation (sometimes referred to as parabolic wave equation) has been used extensively in the hydrocarbon industry primarily as a forward propagator in seismic reflection migration (e.g., Claerbout, 1970) but more recently in many other applications, such as modeling shear-wave splitting as well as frequency dependent anisotropy (see Angus, 2014). The one-way wave equation is computationally more

1 efficient than full waveform solutions (e.g., finite-difference method) and this is  
 2 because it reduces the second-order partial differential wave equation into two first-  
 3 order equations (e.g., Fishmann and McCoy, 1984; Thomson, 1999; Angus, 2014).  
 4 This reduction to first-order with respect to a preferred axis limits one-way wave  
 5 equations to transmission problems, since backscatter is neglected, but allows a  
 6 decrease in several orders of magnitude in computational effort (see Angus 2014 for  
 7 review of one-way wave equations). In this paper, we focus on the wide-angle one-  
 8 way wave equation for 3-D acoustic media derived by Thomson (2005). The wide-  
 9 angle acoustic equation is written as

$$10 \quad \varphi(x_1 + \varepsilon, x_\alpha, p_\alpha; \omega) = e^{[-i\omega P_1 \varepsilon]}(1 + Q\varepsilon)\varphi(x_1, x_\alpha, p_\alpha; \omega), \quad (1)$$

11 where  $\varphi$  is the acoustic wavefield,  $\varepsilon$  is the incremental extrapolation step length in the  
 12  $x_1$  direction,  $x_\alpha$  are the lateral coordinates (i.e.,  $\alpha=2,3$ ),  $\omega$  is frequency and  $p$  is  
 13 slowness. The phase propagator coefficient  $P_1$  is defined as

$$14 \quad P_1(x_1, x_\alpha, p_\alpha) = \left[ \frac{1}{v(x_1, x_\alpha)^2} - (p_\alpha)^2 \right]^{1/2}, \quad (2)$$

15 where  $v(x_1, x_\alpha)$  is the 3D variable acoustic velocity. The transmission coefficient  $Q$  is  
 16 the energy flux term

$$17 \quad Q(x_1, x_\alpha, p_\alpha) = \frac{-\partial_1 P_1}{2P_1}, \quad (3)$$

18 that enables correctly modeling the true amplitude in the presence of strong velocity  
 19 gradients.

20 Although equation 1 can be considered computationally efficient when compared to  
 21 more complete full-waveform methods, such as finite-difference methods, it is still  
 22 computationally cumbersome, especially for 3D media. One of the significant  
 23 computational costs of this algorithm stems from the shuttling between the space and

1 wave number domains (see Thomson, 2005); for many algorithms, this shuttling is  
 2 done via very efficient fast Fourier transforms (FFTs). Improvements can be made by  
 3 implementing theoretical approximations (Ferguson and Margrave, 2005) or by  
 4 manipulating model parameterization (Gazdag and Sguazzero, 1984; Thomson,  
 5 2005).

6 To make the implementation of equation 1 computationally efficient, we make use of  
 7 the velocity model interpolation concept introduced by Gazdag and Sguazzero  
 8 (1984). Specifically, rather than having to compute an FFT at each grid point within  
 9 the computational domain for each extrapolation step, an FFT is performed for an  
 10 integer number of velocities. For each grid point, the wavefield is computed by  
 11 linearly interpolating the wavefields from the nearest velocity values greater than and  
 12 less than the individual grid velocity value. To do this, we introduce an automated  
 13 linear interpolation scheme (Angus, 2014). In this approach, at each  $x_1 + \varepsilon/2$  plane the  
 14 acoustic velocity model is discretized into  $i=(1, N)$  velocities

$$15 \quad V_{min}(x_1 + \varepsilon/2, x_\alpha) \leq V_i \leq V_{max}(x_1 + \varepsilon/2, x_\alpha), \quad (4)$$

16 where  $V_{min}$  and  $V_{max}$  are the minimum and maximum acoustic velocities within the  
 17 chosen velocity model, respectively. Next, the propagator  $P_1$  and transmission  
 18 coefficient  $Q$  are evaluated for each discrete velocity  $V_i$ . Then  $N$  acoustic wavefields  
 19  $\phi_i(x_1 + \varepsilon; \omega)$  are evaluated for each discrete velocity  $V_i$  using the wide-angle equation  
 20 1. Finally, for each lateral  $x_\alpha$  grid point, the complete wavefield  $\phi_i(x_1 + \varepsilon; x_\alpha, p_\alpha; \omega)$  is  
 21 synthesized using the linear velocity wavefield interpolation (LVWI) scheme

$$22 \quad \varphi(x_1 + \varepsilon, x_\alpha, p_\alpha; \omega) = \eta_\alpha \varphi_i(x_1 + \varepsilon; \omega) + (1 - \eta_\alpha) \varphi_{i+1}(x_1 + \varepsilon; \omega), \quad (5)$$

23 when  $V_i \leq V(x_1, x_\alpha) \leq V_{i+1}$ . The linear scaling factor is

1  $\eta_\alpha = \left[ 1 - \frac{V(x_1, x_\alpha) - V_i}{\Delta V} \right]$  (6)

2 and

3  $\Delta V = \left[ \frac{V_{min}(x_1 + \varepsilon/2, x_\alpha) - V_{max}(x_1 + \varepsilon/2, x_\alpha)}{N-1} \right]$ . (7)

### 4 **3. Results**

5 To investigate the accuracy of implementing the automated LVWI scheme (equation  
6 5), we generate a suite of synthetic waveforms through the Horn River Basin velocity  
7 model of Maxwell (2009). Figure 2 shows the 6-layer vertical P-wave velocity model  
8 for the shale-gas reservoir, where the targets for hydraulic stimulation are the  
9 Muskwa and Evie shales. To explore the accuracy of the velocity model interpolation  
10 approach, we compare the travel-time and amplitude predictions from equation 5 for  
11 N=2 to N=7 velocity model interpolations with the exact wide-angle equation  
12 (equation 1). We compare the influence of source frequency for a range of six  
13 dominant source frequencies (50, 100, 125, 150, 250 and 500 Hz) and three source  
14 depths (upper shale at 2399 m, low velocity layer at 2510 m, and high velocity layer  
15 at 2490 m).

16 [Figure 2 here]

17 For all simulations, the wavefield is recorded along a vertical array (128 geophones  
18 spaced 6.3 m vertically) giving an aperture of approximately 800 m. Figure 3 shows  
19 the wavefronts and waveforms for a seismic source located at 2399 m depth and  
20 having a dominant source frequency of 250 Hz. In this figure, it can be seen that as  
21 the number of velocity interpolants (N) increases the level of detail in the computed  
22 wavefield becomes sharper. Specifically, the computed waveforms and wavefield  
23 complexity due to the low and high velocity layers become more distinct and are

1 much closer match to the exact solution as N increases to the total number of  
2 discrete velocities (N=7).

3 [Figure 3 here]

4 The methodology used to compare the exact wide-angle wave equation predictions  
5 with the various velocity model interpolations uses cross correlation to evaluate the  
6 time lag between the primary arrivals. The computed time lag represents the  
7 estimated travel-time error. The amplitude error is calculated after first correcting for  
8 the time lag between the primary arrivals and then computing the maximum  
9 amplitude of the two time-corrected arrivals. The amplitude difference is expressed in  
10 terms of percentage difference from the exact wide-angle maximum amplitude.

11 Figures 4-6 show the results of comparing the exact wide-angle solution with the  
12 LVWI for the 6 velocity model interpolations (N=2 up to N=7. In Figure 4, we compare  
13 the amplitude difference (error) for each velocity model interpolation for the 6  
14 frequencies. Increasing the velocity interpolants from N=2 to N=7 yields improved  
15 amplitude matches as expected. However, as the dominant source frequency  
16 increases so does the general amplitude error.

17 [Figure 4 here]

18 In Figure 5, travel-time differences for each velocity model interpolation with respect  
19 to the exact wide-angle solution are shown for the 6 frequencies. Increasing the  
20 velocity interpolants from N=2 to N=7 yields improved travel-time matches as  
21 expected. For the travel-time predictions, the sensitivity to model interpolant and  
22 source frequency is less severe compared to the amplitude differences shown in  
23 Figure 4. At N=2, the travel-time error ranges between 5 ms and 10 ms, but for N>2  
24 these errors fall below 2 ms regardless of source frequency. It should be noted that  
25 the large travel-time errors computed for the low velocity model interpolant cases are

1 an artifact of the conventional cross-correlation technique used (e.g., Whitcombe et  
2 al., 2010) related to the distorted waveforms (i.e., receivers 90 to 110 in Figure 3)  
3 within the high/low velocity transition zone of the Mid-Devonian Carbonate layer and  
4 the Evie Shale layer.

5 [Figure 5 here]

6 In Figure 6, we compare both the amplitude and travel-time differences for a 150 Hz  
7 dominant source frequency event but located at three different depths; 2399 m within  
8 the Muskwa shale, 2490 within the Mid-Devonian carbonate, which acts as a high  
9 velocity layer, and 2510 within the Evie shale which acts as a low velocity layer (or  
10 wave guide). For all depths, the general trend of improving amplitude and travel-time  
11 prediction with increasing velocity model interpolant can be seen. Furthermore, there  
12 appears to be no significant influence of velocity contrast above and below the  
13 seismic event. Assuming travel-time picking error of 2-3 ms (e.g. Humphries, 2009;  
14 Qiao and Bancroft, 2010; Kocon and van der Baan, 2012), the results from figures 4-  
15 6 suggest a suitable value for model interpolation would be  $N=3$  or  $N=4$ . However, if  
16 accurate amplitude information is required (e.g., for seismic moment tensor  
17 inversion) then  $N>4$  would be necessary.

18 [Figure 6 here]

## 19 **4. Conclusions**

20 We have shown that ray-based approaches are not necessarily always suitable for all  
21 microseismic applications. For instance, eikonal solvers compute very effectively the  
22 first arrival travel-time, regardless of whether this arrival has any energy observable  
23 above the noise. Furthermore, ray based approaches assume any velocity influence  
24 on travel-time is localized along the infinitely thin ray path and hence neglect velocity

1 averaging that bandlimited seismic waves experience. Analysis of the influence of  
2 velocity model uncertainty and source frequency on location accuracy using an  
3 eikonal solver will be biased by the accuracy of the approximate forward propagator  
4 of the eikonal location algorithm. Thus error estimates from ray-based algorithms will  
5 not necessarily convey the true error. No amount of statistical sophistication can  
6 provide accurate error estimates if the forward model is not accurate enough. Thus,  
7 any mislocation will come not only from errors in travel-time picking and velocity  
8 model uncertainty, but also from limitations in the forward model (Green's function)  
9 used in the event location algorithm.

10 In this paper, we have studied the feasibility of using wide-angle one-way wave  
11 equations to compute travel-time and amplitude. Although it is difficult to improve  
12 velocity model uncertainty, we can certainly make improvements in the forward  
13 propagator in location algorithms. Here we examine one approach to achieve  
14 computational efficiency in the wide-angle wave equation and compare amplitude  
15 and travel-time prediction errors to the exact wide-angle solution. The results are  
16 promising considering that further computational and algorithm efficiencies can be  
17 made. Although these results are applied to acoustic media, the results have  
18 implications for wide-angle one-way wave equations for 3D elastic, anisotropic  
19 media.

## 20 **ACKNOWLEDGMENTS**

21 The authors would like to acknowledge the sponsors of the ITF FRACGAS consortium  
22 (Chevron, EBN, ExxonMobil, Marathon Oil, Nexen, Noble Energy and Total) and phases 2  
23 and 3 of the BUMPS consortium (BP, Chevron, CGG, Cuadrilla, ExxonMobil, Maersk Oil,  
24 Microseismic, PDO, Pinnacle, Rio Tinto, Schlumberger, Tesla, Total and Wintershall).

## 25 **References**

26 Akima H., A method of bivariate interpolation and smooth surface fitting for irregularly

1 distributed data points, *ACM Transactions on Mathematical Software* **4**, 148-159, 1978.  
2 Angus, D.A., The one-way wave equation: a full waveform tool for modeling seismic body  
3 wave phenomena, *Surveys in Geophysics*, **35**(2), 359-393, 2014.  
4 Carcione J.S., G.C. Herman and A.P.E. ten Kroode, Y2K Review Article: Seismic modeling,  
5 *Geophysics*, **67**(4), 1304-1325, 2002.  
6 Cerveny V. *Seismic ray theory*, Cambridge University Press, Cambridge, 2001.  
7 Claerbout J., Coarse grid calculations of wave in inhomogeneous media with application to  
8 delineation of complicated seismic structure, *Geophysics* **35**(3), 407-418, 1970.  
9 Eisner L., Williams-Stroud S., Hill A., Duncan P. and Thornton M., Beyond the dots in the  
10 box: Microseismicity-constrained fracture models for reservoir simulation, *Leading Edge*  
11 **29**, 326–333, 2010a.  
12 Eisner, L., Hulseley, B.J., Duncan, P., Jurick, D., Werner, H. and Keller, W., Comparison of  
13 surface and borehole locations of induced seismicity, *Geophysical Prospecting*, **58**, 809-  
14 820, 2010b.  
15 Ferguson R. and Margrave G., Planned seismic imaging using explicit one-way operators,  
16 *Geophysics* **70**, S101–S109, 2005.  
17 Fishmann, L. and McCoy, J. Derivation and application of extended parabolic wave theories.  
18 I. The factorized Helmholtz equation, *Journal of Mathematical Physics*, **25**, 285–296.  
19 1984.  
20 Gazdag J. and Sguazzero P., Migration of seismic data by phase shift plus interpolation,  
21 *Geophysics* **49**(2), 124-131, 1984.  
22 Gibowicz S.J. and Kijko A., *An introduction to mining seismology*, Academic Press, 1994.  
23 Humphries M., Locating VSP diffracted arrivals using a microseismic approach, *SEG*  
24 *Houston International Exposition and Annual Meeting*, 4184-4188, 2009.  
25 Jones, I.F. *An introduction to: Velocity model building*, EAGE Publications, Netherlands,  
26 2010.  
27 Jones, G.A., Kendall, J-M., Bastow, I.D. and Raymer, D.G., Locating microseismic events  
28 using borehole data, *Geophysical Prospecting*, **62**, 34-49, 2014.  
29 Kocon K. and van der Baan M., Quality assessment of microseismic event locations and  
30 traveltimes picks using a multiplet analysis, *The Leading Edge* **31**(11), 1330-1346, 2012.  
31 Larsen S. and Harris D., Seismic wave propagation through a low-velocity nuclear rubble  
32 zone, *Lawrence Livermore National Laboratory*, 1993.  
33 Maxwell, S., *Microseismic imaging of hydraulic fracturing: Improved engineering of*  
34 *unconventional shale reservoirs*, SEG Distinguished Instructor Series, **17**, 2014.  
35 Maxwell, S., Microseismic location uncertainty, *CSEG Recorder*, April, 41-46, 2009.  
36 Price, D., The effect of anhydrite on the surface imaging of microseismic events, *MSc*  
37 *dissertation*, University of Leeds, 2013.  
38 Qiao B. and Bancroft J.C., Picking microseismic first arrival times by Kalman filter and  
39 wavelet transform, *CREWES Research Report* **22**, 2010.  
40 Rentsch S., Buske S., Luth S. and Shapiro S.A., Fast location of seismicity: A migration-type  
41 approach with application to hydraulic-fracturing data, *Geophysics*, **72**(1), S33-S40, 2007.  
42 Sambridge M., Geophysical inversion with a neighbourhood algorithm-I: Searching a  
43 parameter space, *Geophysical Journal International* **138**, 479-494, 1999a.  
44 Sambridge M., Geophysical inversion with a neighbourhood algorithm-II: Appraising the  
45 ensemble, *Geophysical Journal International* **138**, 727-746, 1999b.  
46 Sethian J. and Popovici A., 3-D traveltimes computation using the fast marching method,  
47 *Geophysics* **64**(2), 516-523, 1999.  
48 Sethian J., A fast marching level set method for monotonically advancing fronts, *Proceedings*  
49 *of the National Academy of Sciences of the United States of America* **93**(4), 1591-1595,  
50 1996.  
51 Teanby N., Kendall J-M., Jones R.H. and Barkved O., Stress-induced temporal variations in  
52 seismic anisotropy observed in microseismic data, *Geophysical Journal International*, **156**,  
53 459-466, 2004.  
54 Thomson C.J., The 'gap' between seismic ray theory and 'full' wavefield extrapolation,  
55 *Geophysical Journal International*, **137**, 364-380, 1999.

- 1 Thomson C.J., Accuracy and efficiency considerations for wide-angle wavefield extrapolators  
2 and scattering operators, *Geophysical Journal International* **163**, 308-323, 2005.
- 3 Thomson C.J. and Chapman C.H., True-amplitude wide-angle one-way propagators and  
4 high-gradient zones, *EAGE 68th Conference and Exhibition H045*, Vienna, Austria, 2006.
- 5 Thornton M., Velocity uncertainties in surface and downhole monitoring, *EAGE 4<sup>th</sup> Passive*  
6 *Seismic Workshop PS08*, Amsterdam, Netherlands, 2013.
- 7 Trifu C.I., Angus D.A. and Shumila V., A Fast Evaluation of the Seismic Moment Tensor for  
8 Induced Seismicity, *Bulletin of the Seismological Society of America*, **90**(6), 1521-1527,  
9 2000.
- 10 Usher P.J., Angus D.A. and Verdon J.P., Influence of a velocity model and source frequency  
11 on microseismic waveforms: some implications for microseismic locations, *Geophysical*  
12 *Prospecting* **61**, 334–345, 2013.
- 13 Virieux, J., SH wave propagation in heterogeneous media, velocity-stress finite difference  
14 method, *Geophysics*, **49**, 1259-1266, 1984.
- 15 Virieux, J., P-SV wave propagation in heterogeneous media, velocity-stress finite difference  
16 method, *Geophysics*, **51**, 889-901, 1986.
- 17 Whitecombe, D.N., Paramo, P., Philip, N., Toomey, A., Redshaw, T. and Linn, S., The  
18 correlated leakage method – it's application to better quality timing shifts on 4D data, 72nd  
19 EAGE meeting, Barcelona, Spain, Extended Abstracts, B037, 2010.
- 20

# 1 Tables

2 **Table 1:** Event locations as computed using the eikonal solver. The 3 synthetic datasets were  
3 generated using the 3 velocity models. Travel-time picks for each dataset were then used to locate the  
4 event using the various velocity models (yielding 9 permutations). The relative location of the event is  
5 330 m horizontally (lateral distance from the well) and 750 m in depth.

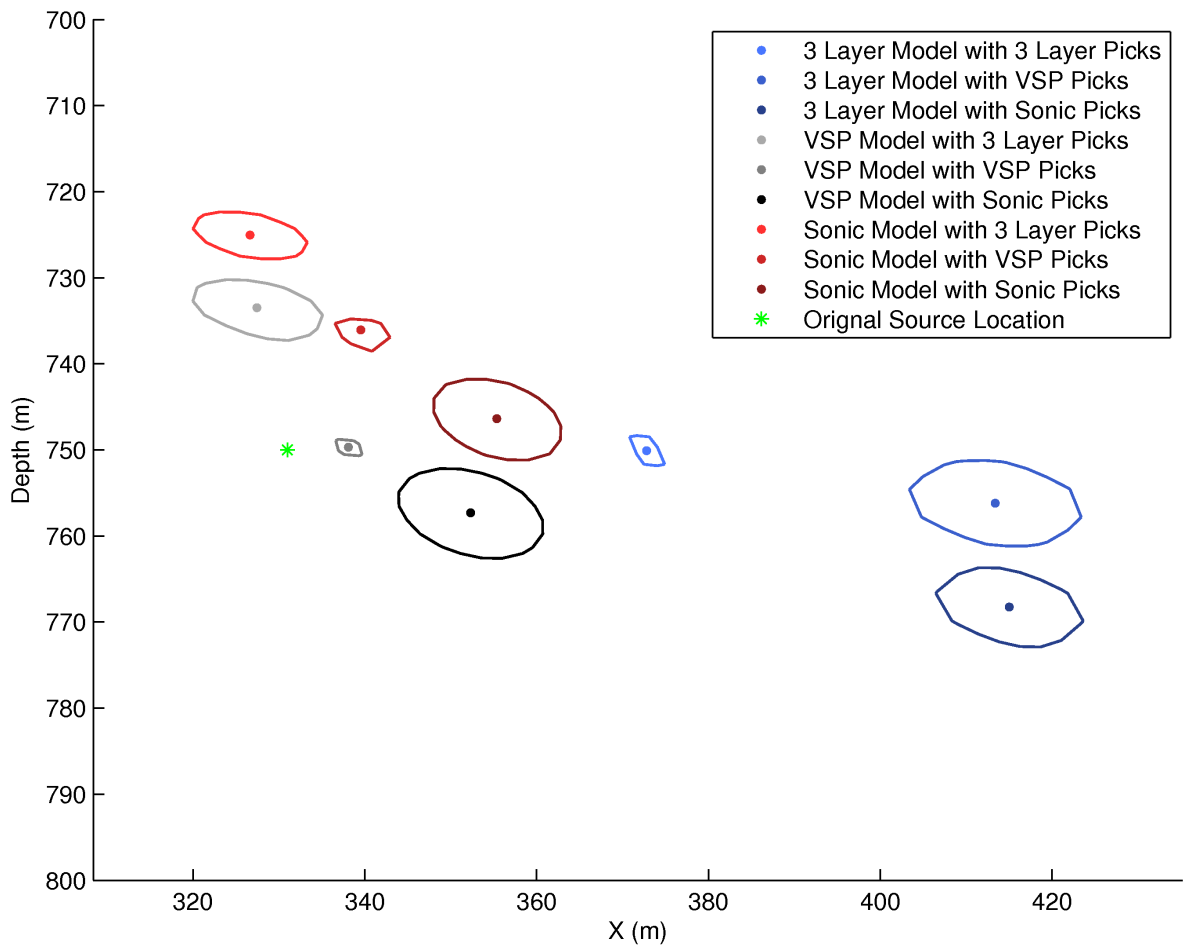
| Velocity model for synthetics | Velocity model for location algorithm |           |             |           |             |           |
|-------------------------------|---------------------------------------|-----------|-------------|-----------|-------------|-----------|
|                               | Sonic                                 |           | VSP         |           | 3 layer     |           |
|                               | Lateral (m)                           | Depth (m) | Lateral (m) | Depth (m) | Lateral (m) | Depth (m) |
| Sonic                         | 355                                   | 746       | 352         | 757       | 415         | 768       |
| VSP                           | 340                                   | 736       | 338         | 750       | 413         | 756       |
| 3 layer                       | 327                                   | 725       | 327         | 733       | 373         | 750       |

6

7

1 **Figures**

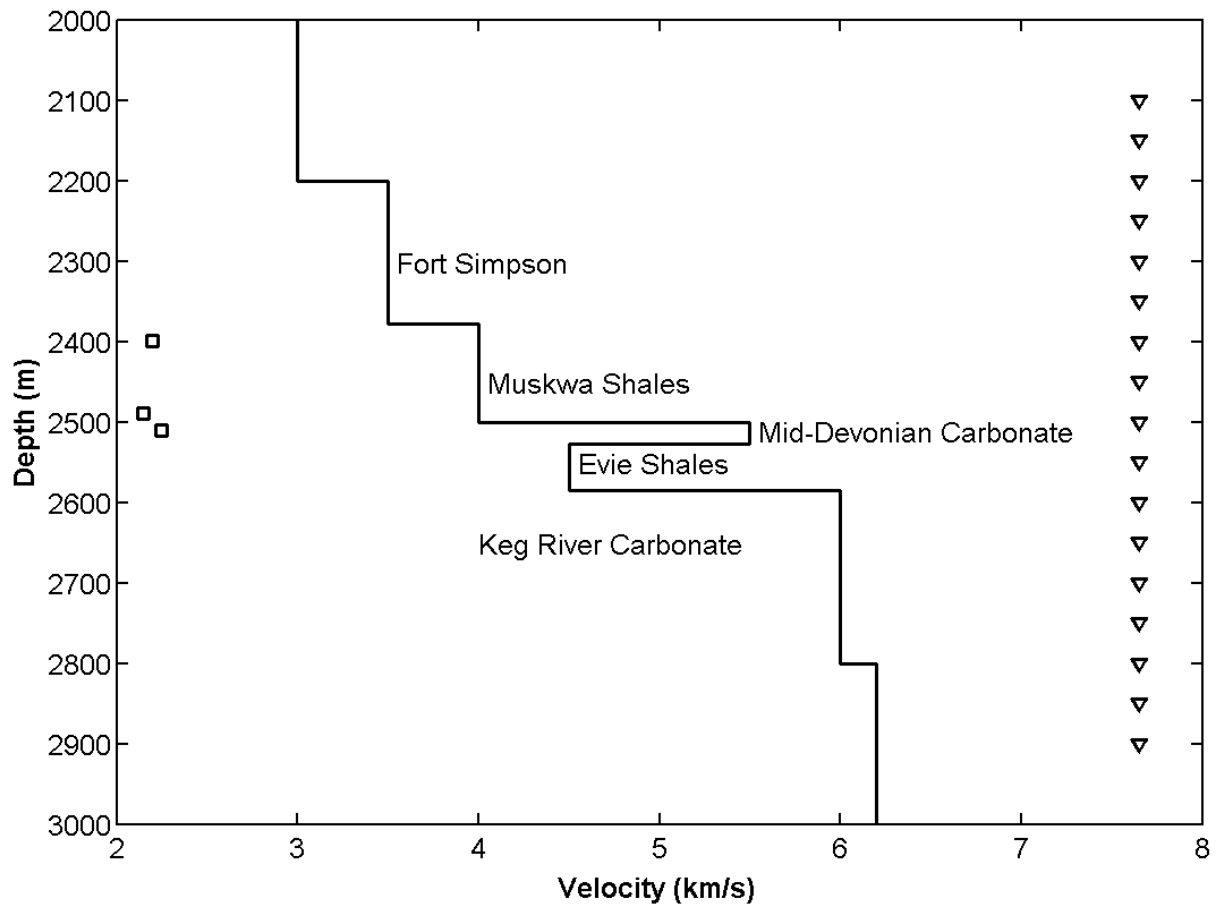
2



3

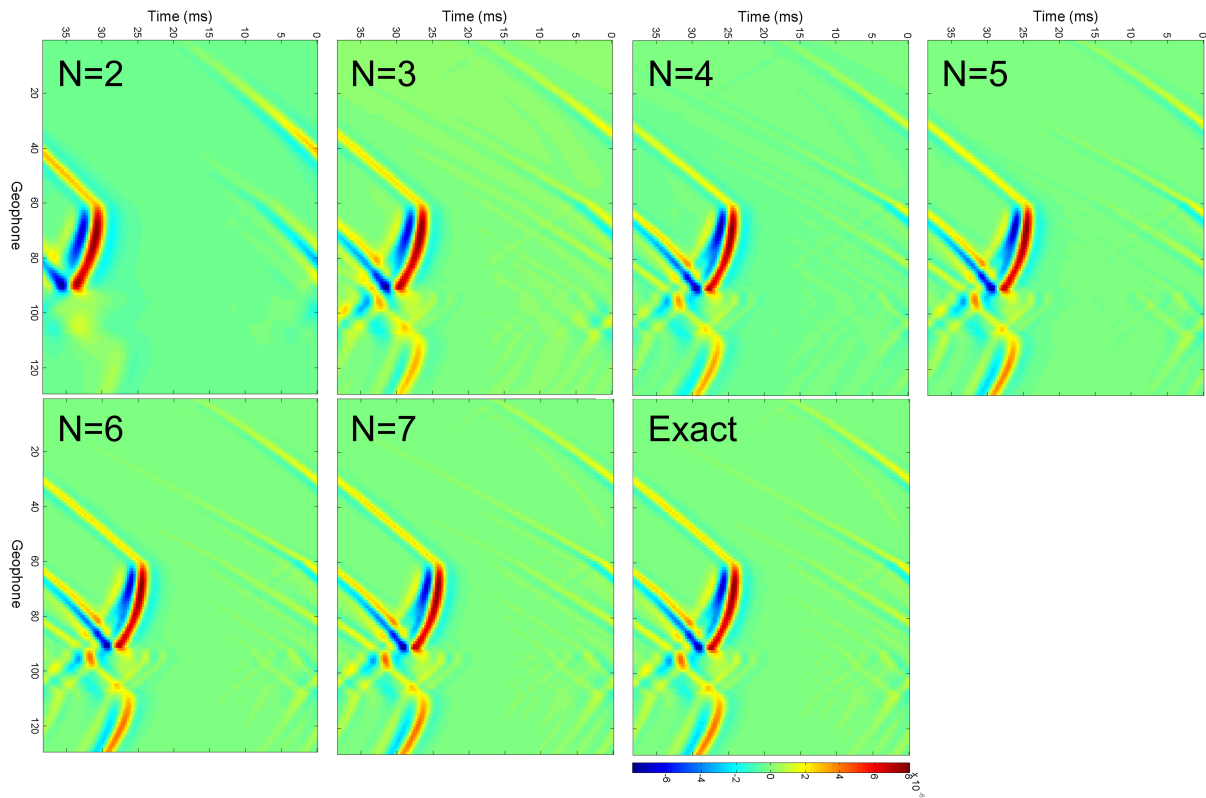
4 **Figure 1:** Comparison of event locations using the eikonal solver with respective 90%  
 5 confidence ellipses for a source with dominant source frequency of 300 Hz. The true source  
 6 location is indicated by the green star. The blue values represent results where the synthetic  
 7 waveforms were generated using the 3-layer velocity model, the grey/black using the VSP  
 8 velocity model and the red using the sonic velocity model. The finite-difference algorithm  
 9 E3D is used to generate the synthetic microseismic data and the travel times from the full-  
 10 waveform finite-difference seismograms are picked manually. The eikonal solver uses the  
 11 finite-difference full-waveform travel time picks to predict the event location.

12



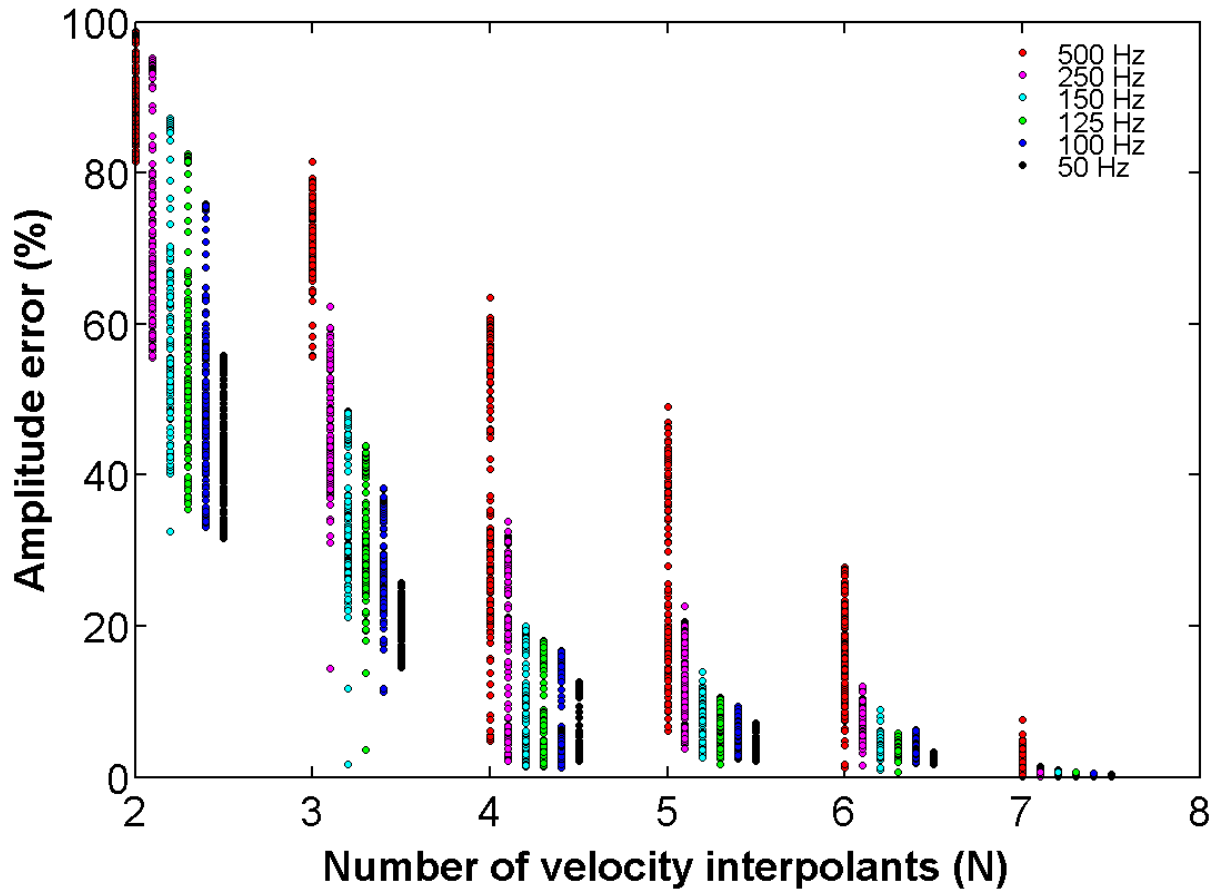
1  
 2 **Figure 2:** P-wave velocity model of the Horn River Basin reservoir used in the wide-angle  
 3 simulations. The square symbols on the left represent the relative depth of the three seismic  
 4 sources. The inverted triangle symbols on the right show the relative depth extent of the  
 5 vertical array consisting of 128 geophones. The lateral distance between source and  
 6 geophone array is 250 m (not shown to scale in this figure).

7

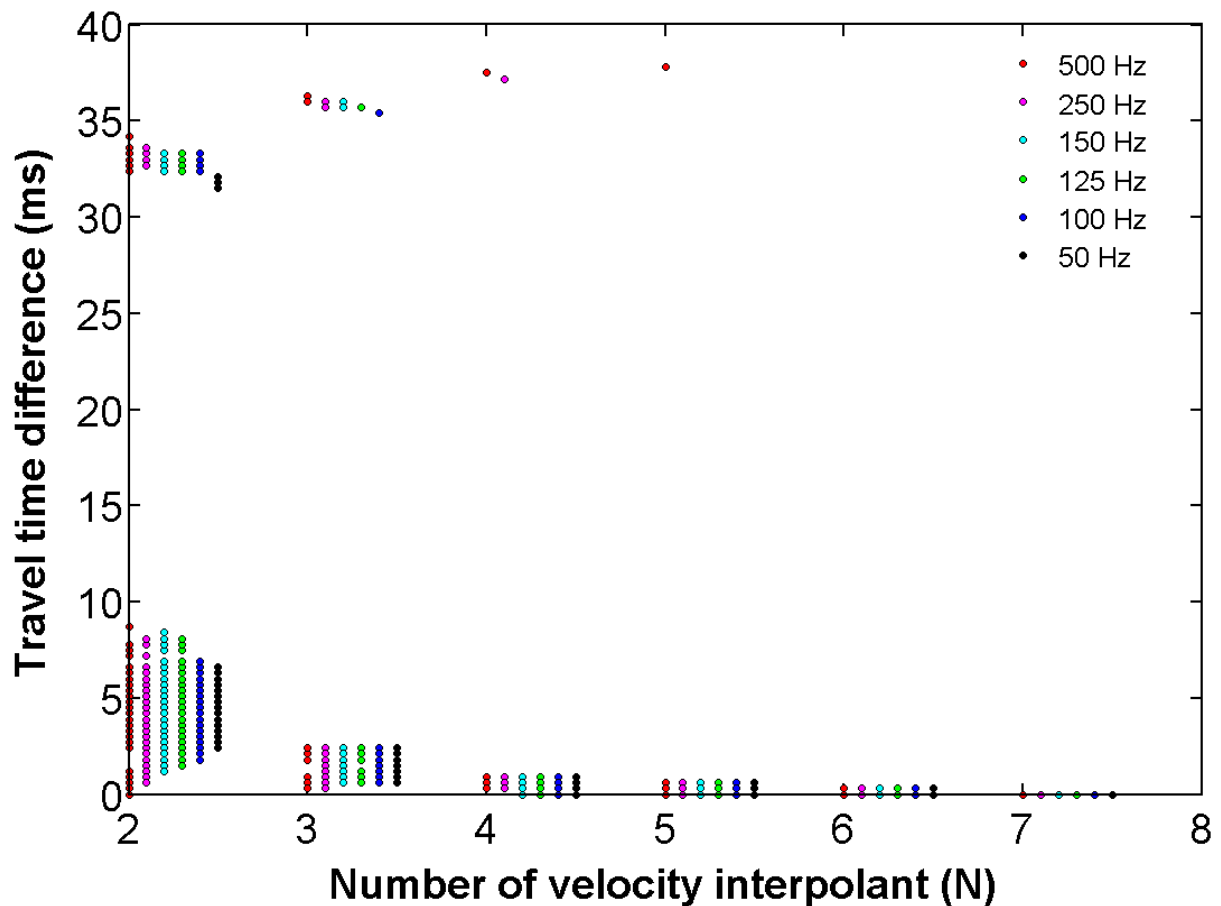


1  
 2 **Figure 3:** Vertical snapshot of wavefield after propagating a total distance of 250 m  
 3 horizontally for N=2, 3, 4, 5, 6, and 7 number of velocity model interpolants, and the exact  
 4 wide-angle solution. Since the time evolution of the wide-angle solution is computed in the  
 5 frequency domain, the wavefield shows wrap-around in the time axis.

6

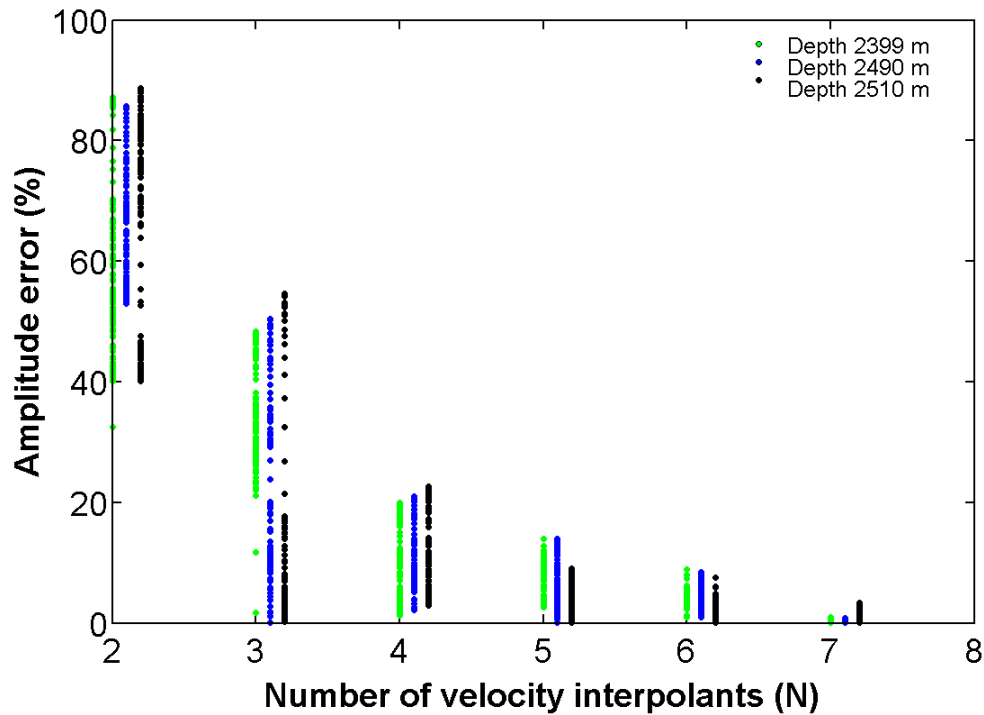


1  
 2 **Figure 4:** Comparison of amplitude error in terms of % difference between the model  
 3 interpolant (N) solution and the exact wide-angle solution for seismic event located at depth  
 4 of 2399 m for all source frequencies.  
 5

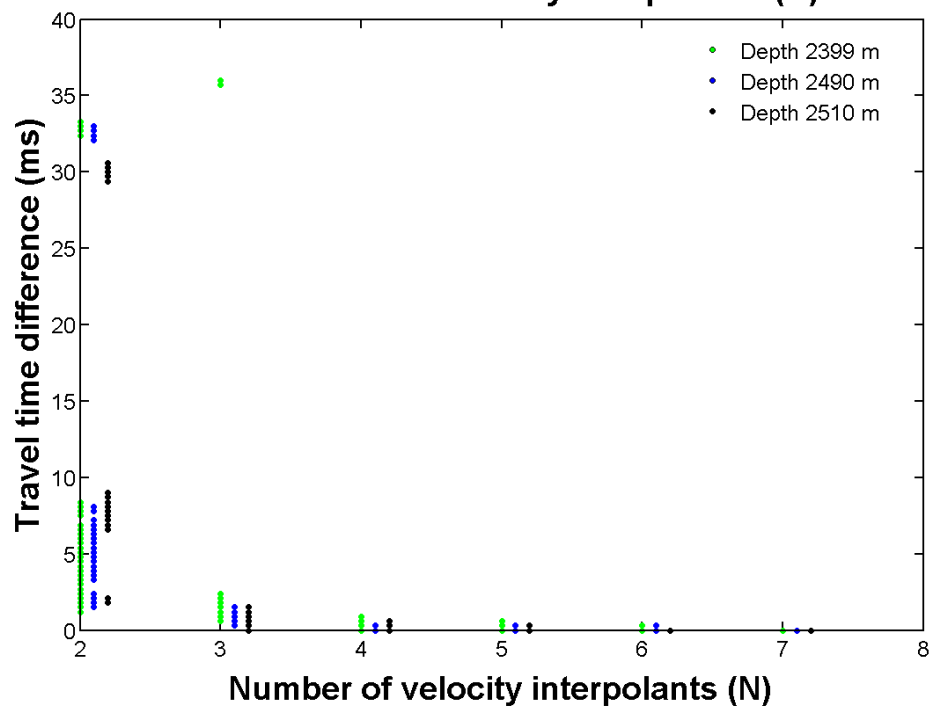


1  
 2 **Figure 5:** Comparison of travel-time error (ms) between the model interpolant (N) solution  
 3 and the exact wide-angle solution for seismic event located at depth of 2399 m for all source  
 4 frequencies. The large travel-time errors (between 30 and 40 ms) are due to inaccurately  
 5 modelled waveforms (i.e., receivers 90 to 110 in Figure 3) within the high-to-low velocity  
 6 transition of the Mid-Devonian Carbonate and Evie Shales (Figure 2). The waveform  
 7 distortion causes noticeable artifacts in the results of the conventional cross-correlation  
 8 technique used.

9



1



2

3 **Figure 6:** Comparison of (top) amplitude error in terms of % difference and (bottom) travel-  
 4 time error (ms) between the model interpolant (N) solution and the exact wide-angle solution  
 5 for seismic event with dominant frequency of 150 Hz.

6

7